Determination of geochemical anomalies and gold mineralized stages based on litho-geochemical data for Zarshuran Carlin-like gold deposit (NW Iran) utilizing multi-fractal modeling and stepwise factor analysis

F. Aliyari[1*], P. Afzal[2] and J. Abdollahi Sharif[3]

1. Department of Mining Engineering, Urmia University of Technology, Urmia, Iran
2. Department of Mining Engineering, South Tehran Branch, Islamic Azad University, Tehran, Iran
3. Department of Mining Engineering, Urmia University, Urmia, Iran

Abstract

The Zarshuran Carlin-like gold deposit is located at the Takab Metallogenic belt in the northern part of the Sanandaj-Sirjan zone, NW Iran. The high-grade ore bodies are mainly hosted by black shale and cream to gray massive limestone along the NNE-trending extensional fault/fracture zones. The aim of this investigation was to determine and separate the gold mineralized stages based on the surface litho-geochemical Au, Hg, and As data using the Concentration-Area (C-A) fractal model and stepwise factor analysis in the Zarshuran gold deposit. Three mineralized stages were determined by the C-A fractal modeling and factor analysis, which were correlated with the mineralized stages from geological studies. The main stage of Au mineralization was higher than 1.995 ppm, which was correlated with the main sulfidation stage, whereas the As and Hg highly intense anomalies (higher than 6409 and 19 ppm, respectively) were associated with the quartz-sulfide veins and veinlets. The results obtained by the C-A fractal model and stepwise factor analysis showed that the main gold mineralized stage occurred in the southern part of the Zarshuran deposit, which was correlated with the geological particulars.

Keywords: *Litho-Geochemical Anomaly, Concentration-Area Fractal Model, Stepwise Factor Analysis, Zarshuran.*

1. Introduction

The Zarshuran sedimentary rock hosting the Carlin-like gold deposit (SRHGD) is located at the Takab Metallogenic belt in the northern part of the Sanandaj-Sirjan zone, NW Iran (Figure 1a). The N-NW-trending Takab structural belt hosts several middle Miocene magmatic systems and the related world-class epithermal gold deposits such as Zarshuran [1-3], Sari Gunay [4, 5], and Aghdarreh [3, 6]. The exploration history of gold prospecting in the Zarshuran area commenced a hundred years ago based on orpiment and realgar mining in the Takab area [7]. Systematic exploration in the Zarshuran deposit began in the 1990s by the BHP Co and Ministry of Mines and Metals of Iran, and then continued by the Anglo American Exploration and Minorco Co from 1996

to 2003. Several aspects of exploration including the geology, geochemistry, and geophysics were carried out by Geological Survey of Iran, Mineral Export Co, Minor Co, and Anglo American Exploration Co. Detailed explorations were also continued towards the peripheral parts to determine the extent of high-grade ore bodies in the lateral portions. The studies have shown that the Zarshuran gold deposit contains an estimated resource higher than 80 t Au with average grades between 3 and 4 g/t Au [3]. However, the final reserve estimation using the 3D geostatistical methods on 47 drill core data and resource classification by JORC standard in the Zarshuran gold deposit indicated a resource of 100 t Au at grades of 4.24 g/t Au [8, 9].

Several investigations including the geology, genesis, and nature of the ore-forming fluids [1, 2, 10, 11], remote sensing, geophysics, and genesis of high grade ore bodies [12], and mineralogy of ore-stage paragenesis have been carried out at the Zarshuran gold deposit [3, 6]. However, the roles of the major tectono-deformational events, magmatism, ore controls, potential source rock for gold mineralization, overall sources for fluids and metals, and timing of gold mineralization are still the matters of debate. Furthermore, previous studies did not address the regional geochemical anomaly detection and delineation of the mineralization stages using the litho-geochemical data.

The fractal geometry established by Mandelbrot (1983) [13] is a non-linear one, and has been widely applied in geosciences [13-33]. Cheng et al. (1994) [16] have proposed the Concentration–Area (C–A) fractal model for delineation of different geochemical populations, especially for hydrothermal deposits that have been an evolution in the geochemical studies for determination of various elemental anomalies and related mineralized stages from background. Fractal dimensions in geological and geochemical processes correspond to the variations in physical characteristics such as lithology, vein density or orientation, fluid phase, alteration phenomena, and structural feature or dominant mineralogy [18]. Heidari et al. (2013) [33] have used the C-A model for separation of mineralized stages in the Touzlar gold deposit.

Multivariate methods are proper for that aim because the relative importance of the combinations of geochemical variables can be evaluated. Additionally, the ore element with its paragenesis is modeled in geochemical explorations, which have been widely used for interpretation of the stream sediment and lithogeochemical data (e.g. [34-38]). The main purpose of factor analysis is to describe the variations in a multivariate dataset (values of different elements in this study) by a few factors as possible and to detect the hidden multivariate data structures for determination of elemental paragenesis [39]. The stepwise factor analysis proposed by Yousefi et al. (2012) [38] is an applicable method for a better generation of the

factors that could be the separation of paragenesis elements in different types of ore deposit.

The main aim of this work was to determine and delineate various mineralized stages in the Zarshuran deposit using the C-A fractal model and stepwise factor analysis. Moreover, fractal modeling was used for the results derived via the stepwise factor analysis, and correlated with geological modeling for delineation of the stages and sub-stages of gold mineralization in the Zarshuran deposit. Furthermore, the hybrid modeling implicated using paragenesis of Au for recognition of the gold mineralized stages in the area. The results obtained by the multi-fractal modeling and stepwise factor analysis were correlated with the geological particulars in this deposit.

2. Geological setting
2.1. Regional geology and stratigraphy
The Takab Metallogenic Belt (TMB) consists of allochthonous rock formations that are formed in an active continental margin. The geotectonic history of TMB is characterized by the subduction and accretion events accompanied by periodic deformation, plutonism, volcanism, and reorientation of structural features [41-43].

Rock units in the area are comprised of three stratigraphic groups including Jangutaran, Chaldagh, and AmirAbad [40]. The age of these sedimentary successions ranges from Neoproterozoic to early Paleozoic, and the dominant lithologies are metamorphosed and deformed massive to thick-bedded limestone, black shale, siltstone, and conglomerate together with tholeiitic to calc-alkaline mafic and bimodal flows and volcanoclastics. The high angle N-NE- and NW-trending strike-slip faults may have played a major role during the sediment deposition and evolution of the basin [2, 11].

TMB comprises several large deposits/occurrences including the Zarshuran Au-As and Aghdarreh Au-Sb-Hg deposits [1-6], Touzlar Au-Ag (Cu) [44, 33], Anguran Zn-Pb deposit [45-48], Bayche Bagh Cu-Ni-Co deposit [49-52], and other numerous unknown small deposits/occurrences (Figure 1b).
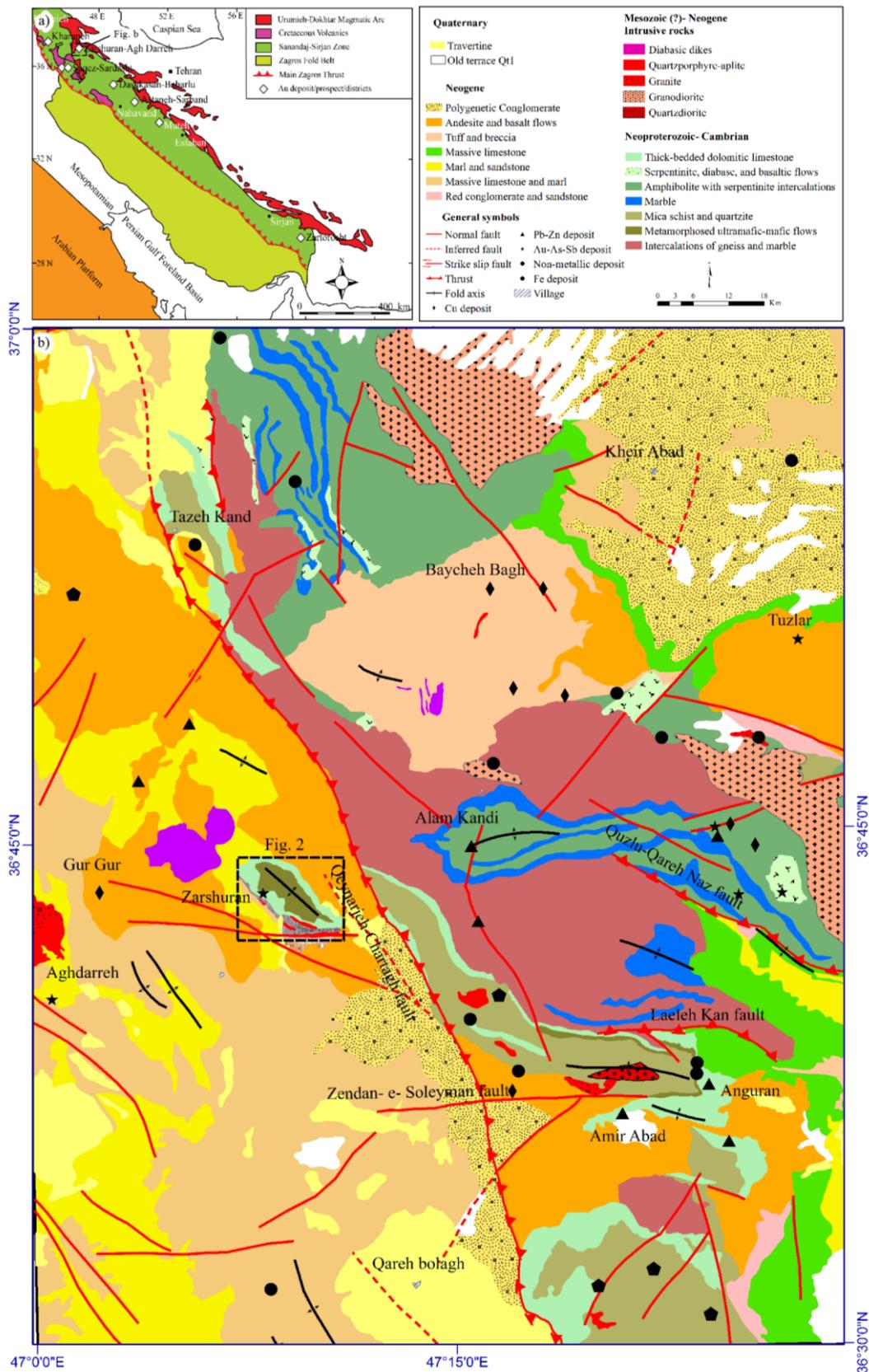
Figure 1. a) Location of Zarshuran-Aghdarreh and other Iranian gold deposits in Sananndaj-Sirjan zone; b) Schematic regional geological map of Takab-Zanjan area, NW Iran, showing major tectonic units, volcano-sedimentary sequences, and location of major deposits/occurrences (Modified from Babakhani, A. and Ghalamghash, J. (1990) [40]).

2.2. Deposit geology

The Zarshuran gold deposit exhibits the metamorphosed siliciclastic and carbonate rocks of Neoproterozoic to early Paleozoic age, volcanic rocks of Tertiary age, and sedimentary units of Quaternary age (Figure 2). These rock units consist of the metamorphosed Iman Khan Complex, Chaldagh metalimestone, Zarshuran black shale, and recrystallized limestone, mostly assigned to the Neoproterozoic to early Paleozoic. The Iman Khan Complex consists of an up to 500-m-thick sequence of deep green to greenish gray, mylonitic sericite-chlorite-serpentine-quartz schist. This complex comprises highly metamorphosed and deformed oldest rocks and strata in outcrops and drill cores (Figure 2). In addition, the Iman Khan Complex thrust upon and mostly contain tectonic slices of carbonate and siliciclastic (calc schist) rocks. The carbonatic Chaldagh rock unit comprises laminated, thick-bedded to massive, non-fossiliferous, locally argillaceous limestone, wackstone, and local packstone (Figure 2). The unit ranges from 100 to 200 m in thickness, and varies from dark gray to black to creamy to buff colored in unaltered outcrops.

The Zarshuran Black Shale with more than 150 m thickness conformably overlies the Chaldagh sequence. It is typically composed of an organic-rich, pyritic, locally graphitic black to dark gray carbonaceous shale to siltstone with fine-grained greywacke interbeds (Figure 2). The Zarshuran black shale is a moderately to intensely metamorphosed unit, and fragmented with high angle, normal faults, brecciated, and clast-in matrix textures. It also hosts the gold ores, especially along horizons of increased permeability such as calcite- and debris flow-rich parts. The recrystallized limestone includes an up to 100-m-thick sequence of pink to brown, metamorphosed, medium- to thick-bedded, argillaceous dolomitic limestone.

These rocks are typically metamorphosed and silicified but do not comprise the host units for the mineralized zones. These sedimentary rock units strike NW (~45°) and dip gently NE at an average 25 to 35° with minor changes in dip that could be attributed to dissolution collapse during hydrothermal alteration (Figure 2).

High-angle faults with normal intersections can be divided into two sets based upon cross-cutting relationships and stratigraphic displacements (Figure 2). These structures vary from NW- to NE-trending that offset the Neoproterozoic to lower Paleozoic rocks. It seems that the E-NE-trending high-angle normal faults are the youngest structures in the Zarshuran mining area. Moreover, there is an E-W trending fault system that inferred to be older and deeper than the former structures.

Neogene igneous rocks including the volcanic rocks, flows, tuffs, and intrusive bodies were emplaced episodically during the igneous activity of TMB [4]. The felsic to intermediate volcanic rocks form a locally distributed sequence of sparsely porphyritic lava flows that conformably overlies the Neoproterozoic to early Paleozoic sequences. The units range from andesitic to trachy andesitic porphyry, weakly propylitically (chloritized) altered flows and tuff, 30 to 100-m-thick, were erupted in the southern part of the district.

The Miocene to Pliocene microdiorite, ranging in thickness from 50 to 100 m, cross-cuts the metamorphosed limestone and siliciclastic rocks. This unit is grayish white with a slight rusty coating on weathered surfaces and greenish gray in fresh surfaces and drill cores. This unit is dominantly composed of quartz phenocrysts and plagioclase with a lesser amount of biotite and muscovite. The unit was affected by intense argillic and sericitic and moderate chloritic alteration. Although the microdiorite appears to be magmatic in nature, it distinctly follows a specific horizon that is traceable on surface outcrops and drillcores. The volcanic and plutonic units are distinguished by mildly alkaline (high K) geochemical affinity and Miocene to Pliocene in age that was attributed to a collisional tectonic setting [6]. Quaternary travertine conformably overlies all older sequences and forms a narrow outcrop in the upper central parts of the district.

2.3. Hydrothermal alteration and gold mineralization

Hydrothermal alteration associated with gold mineralization in the Zarshuran deposit consists of decalcification, argillisation, silicification, sulfidation, and, to a lesser extent, alunitization along high-angle normal faults and stratigraphic conduits. The Chaldagh argillaceous limestone is predominantly affected by decalcification along the high-angle normal faults and bedding plane. In the decalcified zones, hydrothermal quartz is absent or is a minor constituent. Black fault gouge, which is mostly composed of dark gray Chaldagh limestone and Zarshuran carbonaceous black shale, is intensely decalcified and correlates with high-grade gold ore. In addition, calcite is entirely removed in intensely decalcified

alteration zones, and therefore, Chaldagh limestone is more argillaceous. The gradual removal of carbonate resulted in the formation of widespread open spaces within the host carbonate rocks and subsequent crystallization of euhedral quartz into spaces created by the decarbonatization process. Therefore, the presence of euhedral quartz, particularly in the upper parts of the altered zones, indicates that the silicification occurred after the decarbonatization and argillic alteration.

Fault-controlled jasperoid (pervasive silicification) is commonly brecciated, is well-developed in the central parts of the orebody, and is strongly correlated with high Au grades. Near the high-angle normal faults, the intensely silicified zones (jasperoid) generally represent the Au grades ranging from 1 to 50 ppm, which gradually decreases distal to these faults. The brecciated texture of jasperoid together with the higher gold contents may imply that these zones are formed from solution collapse along feeder faults during mineralization. Furthermore, the presence of gold-rich brecciated jasperoid

indicated that the high-angle normal faults were active during the hydrothermal alteration and the subsequent gold mineralization. Three main assemblages of hydrothermal sulfide minerals have been recognized in the Zarshuran gold deposit (Table 1; [2]): (I) Early-assemblage, pyrrhotite, pyrite, and chalcopyrite. Low concentrations of gold occurred within the pyrite at this stage. (II) Middle-assemblage, zoned euhedral to subhedral arsenical pyrite, sphalerite, galena, chalcopyrite, and lead-zinc sulfosalts. Major gold concentrations occurred within this assemblage, particularly together with arsenical pyrite. (III) Late-assemblage, network arsenical pyrite, colloform and massive arsenical pyrite, colloform sphalerite, coloradoite, orpiment, realgar, cinnabar, stibnite, getchelite, and As-Sb sulfosalts [53]. The second major gold concentrations occurred as solid solutions or as nanometer-sized native gold in arsenical pyrite and colloform sphalerite of this assemblage. Hydrothermal quartz and orpiment-realgar rarely contains metallic gold (Table 1).
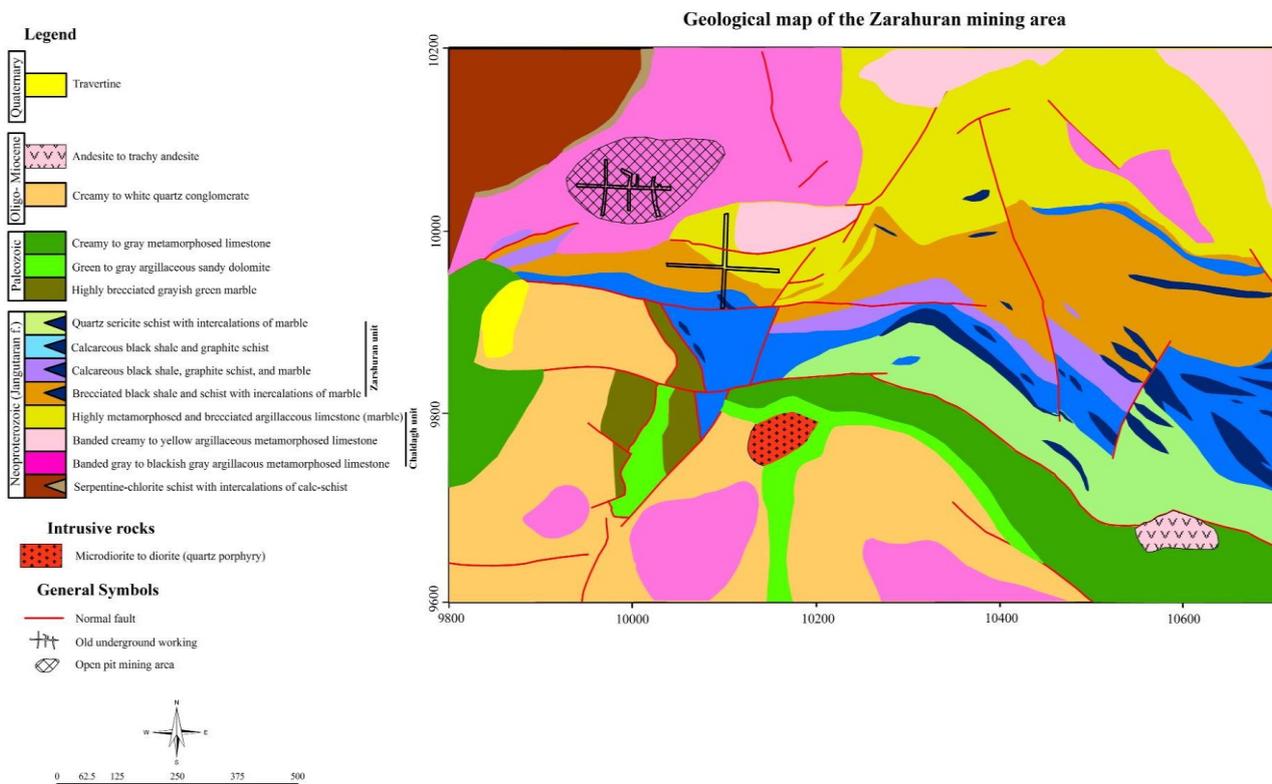
Figure 2. Simplified geologic map of Zarshuran mining area showing various rock units and location of underground and open pit mining area on map (Modified form Madan Kav Co., 2002).

Table 1. Major hydrothermal stages for Zarshuran gold deposit including paragenesis of minerals in preore, gold ore, late gold ore, and postore stages.

	Hydrothermal alteration				
	Pre-mineralization		Mineralization		Post-mineralization
	Stage I	Stage II	Stage I	Stage II	
Hydrothermal stage	Decalcification and argilisation	Euhedral quartz and arsenical pyrite precipitation	Silicification and sulfidation	Silicification and sulfidation	
Ore related textures	-	Disseminated ore textures	Veins and massive ore textures	Veins, veinlets, and Breccias textures	Veinlets and comb textures
Ore minerals	-	Arsenical pyrite	Pyrite, pyrrhotite, and chalcopyrite	zoned euhedral to subhedral arsenical pyrite, sphalerite, galena, chalcopyrite, and lead-zinc sulfosalts, invisible gold	network arsenical pyrite, colloform and massive arsenical pyrite, colloform sphalerite, coloradoite, orpiment, realgar, cinnabar, stibnite, getchelite, and As-Sb-Hg sulfosalts

Gold mineralization at the Zarshuran deposit is primarily lithologically-structurally controlled, and is best developed where those structures intersect favorable host lithologies, specifically Chaldagh metalimestone and Zarshuran black shale. The high grade orebodies are mainly hosted by black shale and cream to gray massive limestone along the NNE-trending extensional fault/fracture zones. The high grade orebody is characterized by a zone of jasperoid breccias and black gouge, and varies from 800 to 1250 m in length, 50 to 80 m in width, and 300 m in thickness. The jasperoid breccia mainly consists of angular to subrounded clasts from a few millimeters to several centimeters of jasperoid with a matrix of quartz, calcite, barite, pyrite, and iron oxide minerals. Therefore, a high-grade portion of the Zarshuran deposit was hosted by the jasperoid breccias [54].

The main orebody consists of an approximately 65% oxidized ore and 35% unoxidized (carbonaceous) [1]. The oxidized ore is spatially associated with both decalcified and silicified zones, whereas the unoxidized ore is mainly associated with the decalcified and arsenide zones. Sulfide minerals, predominantly pyrite and arsenical pyrite, are oxidized into iron oxide minerals, and carbon is remobilized within the oxidized ore. The average grade of unoxidized carbonaceous ore (16 ppm) is higher than the oxidized ore (avg. 9 ppm).

3. Methodology
3.1. C-A multi-fractal model
Cheng et al. (1994) [16] have proposed the concentration–area (C–A) fractal model, which may be utilized to delineate the geochemical

anomalies and the background that has the general form:

$$A(\rho \leq \upsilon) \propto \rho^{-a1} \; ; \; A(\rho \geq \upsilon) \propto \rho^{-a2} \qquad (1)$$

where $A(\rho)$ indicates the area with concentration values greater than the contour value ρ; υ represents the threshold; and a1 and a2 are the characteristic exponents. The two approaches used to calculate $A(\rho)$ by Cheng et al. (1994) were (1) $A(\rho)$ is the area enclosed by the contour level ρ on a geochemical contour map resulting from interpolation of the original data utilizing geostatistical methods, and (2) $A(\rho)$ are the values obtained by box-counting of the original elemental concentration values. By box-counting, one superimposes a grid with cells on the studied area. The area $A(\rho)$ for a given ρ is equal to the number of cells multiplied by the cell area with concentration values greater than ρ.

The breaks between straight-line segments on the C-A log-log plot and the corresponding values of ρ have been used as thresholds to separate the geochemical values into different components, representing different causal factors such as lithological differences and geochemical processes [55]. A correlation between the results obtained by the C-A model with the geological, geochemical, and mineralogical information could be used to define the different mineralized stages in different types of ore deposits, especially the hydrothermal deposit [19, 33].

The multi-fractal theory may be interpreted as a theoretical framework that explains the power-law relations between the areas enclosing concentrations below a given value and the actual concentrations itself. In order to demonstrate and prove that data distribution has a multi-fractal nature requires a rather extensive computation

[56, 57]. An investigation by Bolviken et al. (1992) [58] has shown that the concentration distributions of different elements mostly satisfy the properties of a multi-fractal function. There are some evidences that geochemical distributions are fractal in nature and behavior. Some approaches seem to support the idea that the geochemical data distributions are multi-fractal, although this point is far from being proven [19, 26, 32, 59, 60]. This idea may provide and help the development of an alternative interpretation validation and useful methods to be applied to the elemental geochemical distributions analysis.

3.2. Stepwise factor analysis

The stepwise factor analysis proposed by Yousefi et al. (2012) [38] is based upon the ln- and ilr-transformation that has been developed based on the principal component analysis (PCA) for extraction of factor varimax rotation of factors but it is a multi-step factor analysis to extract the components showing anomalies in multi-element ore deposit-type-based mineralized stages and ore elements. The use of stepwise factor analysis enhances recognition of anomalous geochemical signatures, increases geochemical anomaly intensity, and increases the percentage of the total explained variability of data [38].

4. Litho-geochemical data analysis

The geochemical samples were collected from surface outcrops by the litho-geochemical survey carried out by the IMIDRO (Iranian Mines and Mining Industries Development and Renovation Organization) since 1998 (Figure 3). The chemical analysis of 1627 rock samples collected from 68 profiles across 40 km^2 was used to distinguish the district-scale elemental anomalies in the Zarshuran Carlin-like gold deposit. The sampling density is in the order of one per 200 square meters, which is typical for regional to deposit-scale geochemical survey.

All samples were routinely analyzed for Au and other paragenetic elements using the Inductively Coupled Plasma-Optical Emission Spectrometry (ICP-OES) method for 42 elements in the Laboratory of Iran Mineral Processing Research Center (IMPRC). The detection limits for Au, Ag, As, Sb, Cu, and Hg were 0.001, 0.1, 0.5, 0.5, 1.0 and 0.2 ppm, respectively.

Out of the elements determined by IMPRC, only four elements including Ag, As, Sb, and Hg were selected for mapping significant anomalies based on the type of ore deposit. Au, Ag, and Hg are good indicators for ore element mineralization, and As is a pathfinder element for Carlin-like gold deposits. Therefore, statistical analysis was carried out on the Au, Ag, Hg, and As in the area, which showed that the Au, Ag, As, and Hg mean values were 270 ppb, and 1.32, 1242, and 2.4 ppm, respectively (Table 2). The elemental histograms showed that there were no normal distributions for Au, Ag, Hg, and As (Figure 4), which means that their median could be equal to their threshold values [61]. This is based upon the classical statistics methods, which are related to the normal distribution of data. If the data had a normal distribution, the threshold values for different anomalies could be calculated by summation of average with coefficients of standard deviation. Otherwise, median of the data assumes as the threshold value for anomaly [17, 37, 61]. The median of Au, Ag, Hg, and As were 20 ppb, and 0.6, 1, and 564 ppm, respectively.

5. Application of stepwise factor analysis

The principal component analysis (PCA) was utilized for extraction of factors based on the 42 ln-transformed elemental grade data, and also the varimax rotation of factors was applied by the SPSS software. A third-step factor analysis was used to extract the components illustrating the anomalous multi-element geochemical signatures of the deposit-type sough [62, 63-66]t. In the first step, the factor analysis yielded nine rotated components, each with eigenvalues greater than 0.6 (Table 3). In the second step, some elements were rejected, which were not in the any factor, and consisted of Cd, Cu, Ge, Mo, P, Sb, Sn, Sr, Te, and U, and the factor analysis was carried out on the other elements. In the third step, seven factors were determined with the following groups, as shown in Table 3:

(1) Al, Be, Ce, Bi, Ga, In, K, La, Li, Nb, Rb, Sc, Se, Ta, Th, Ti, V, Yt, and Zr (2) Co, Cr, Fe, Mg, and Ni, (3) Ba, Mn, and Tl (4) Au, As, and Hg (5) Ag and Pb (6) Ca (7) Na.

The third group including Au, As, and Hg are important in the area for mineralization, as shown in factor 4 (F4-3). This association could imply that the gold mineralization occurred at low temperatures, and that As and Hg were the best pathfinder elements in the Zarshuran Carlin-like gold deposit. For a better illustration of the extracted factors, the factor plots in rotated space are shown in Figure 5.
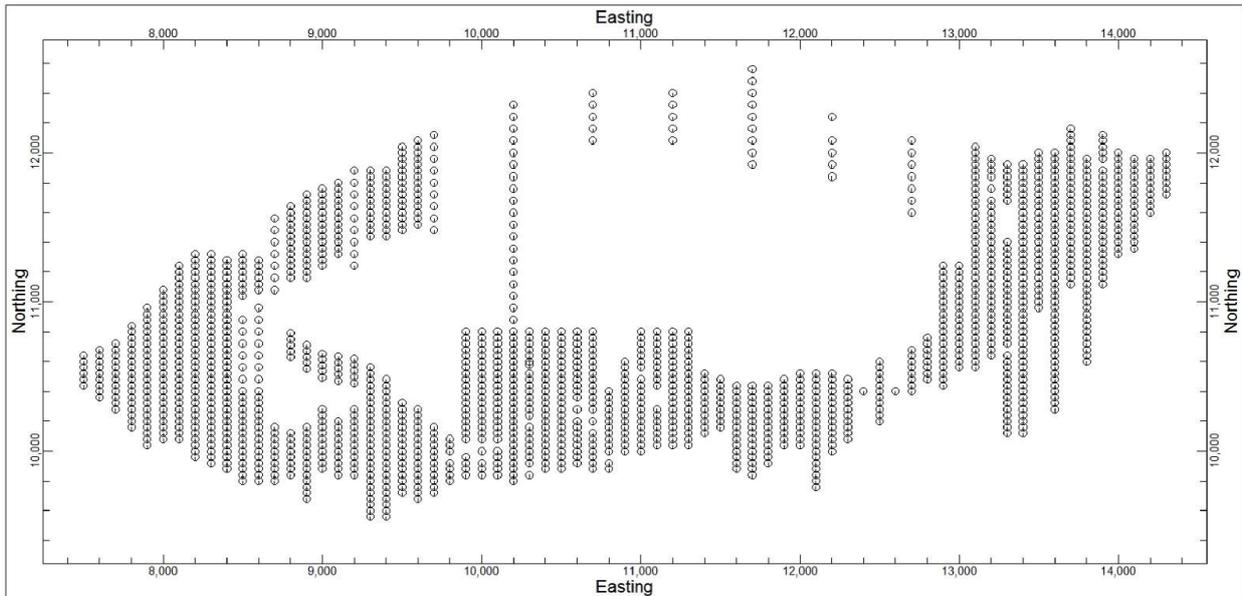
Figure 3. Location map of 1627 litho-geochemical rock samples collected from 68 profiles in a 200 square meteres network across 40 km^2 in Zarshuran area.
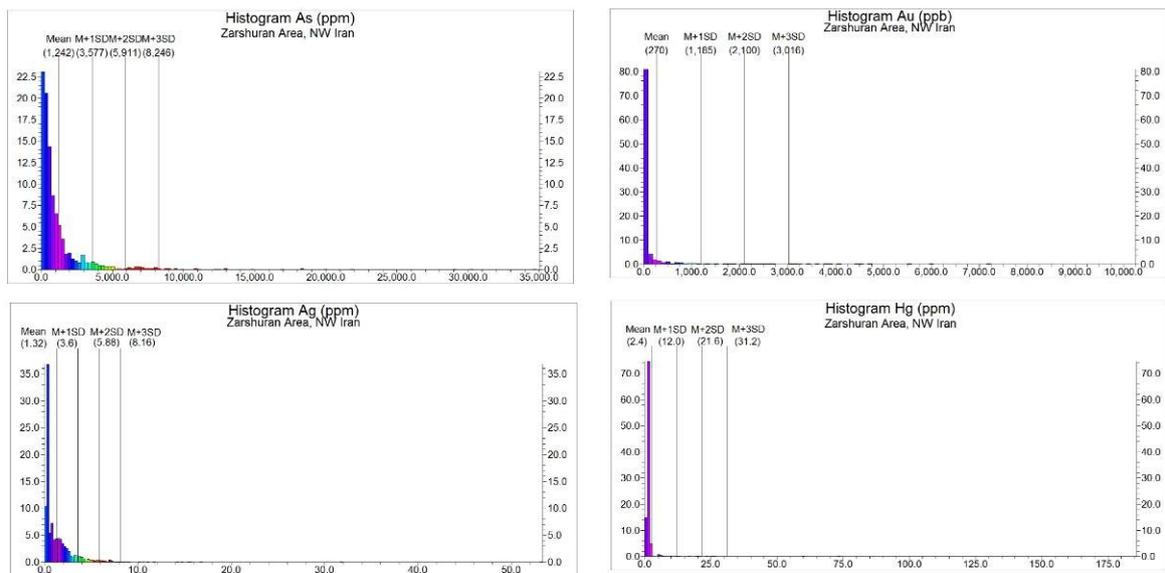
Figure 4. Abundance histograms of Au, Ag, As, and Hg litho-geochemical data from Zarshuran deposit.

Table 2. Statistical characteristics of Au, Ag, As, and Hg based on litho-geochemical samples.

Element	Mean	Median	Maximum	Minimum	SD[*]
Au (ppb)	270	20	10161	0	915.43
Ag (ppm)	1.32	0.6	53.2	0.075	2.28
As (ppm)	1242	564	34785	0.075	2334.56
Hg (ppm)	2.4	1	185	0	9.58

*SD: Standard deviation

6. Application of C-A multi-fractal model

The elemental and F4-3 distributions were recognized by the C-A multi-fractal IDW modeling in the Zarshuran area using the RockWorks™ 15 software package. The IDW method, as a moving average estimation method, was used for estimation of the Au grade in the gridding cells of the area for multi-fractal modeling. In the C-A multi-fractal IDW model, weights for moving average are assigned on the

basis of the local scaling property of the data that is quantified by a power–law function [17, 67]. The area was gridded by 50×20 m cells (100-m-wide squares) based on geochemical sample and factor contouring on logarithmic values that applied an inverse distance weighting option. Therefore, grid cells were identified based on the geometrical properties of the studied area (e.g. distribution of hydrothermal alteration and mineralized lenticular orebody along normal faults) and grid sampling dimensions [68]. The geometrical shapes of the mineralized zones are anisotropic, and the size of gridding dimensions is half of grid sampling in the X and Y dimensions. The C–A log–log plots were generated based on the reverse relationships between the Au, As, Hg, and F4-3 concentrations and their areas, as revealed in Figure 6.

Table 3. Three steps of factor analysis in Zarshuran area: loadings in bold represent selected factors based on threshold of 0.6 in factors.

Rotated component matrix in first step.

	Component								
	1	2	3	4	5	6	7	8	9
Au	-.234	-.002	-.086	-.047	**.675**	.307	-.083	.294	-.013
Ag	.124	-.042	**.789**	.141	-.018	.080	.125	.057	-.106
Al	**.952**	-.135	-.002	.027	-.098	-.022	-.063	-.001	.070
As	-.245	-.007	.135	.190	**.811**	.044	.035	.226	.002
Ba	.137	.031	.131	**.695**	.037	.029	.299	-.042	-.087
Be	**.694**	-.227	-.042	.087	.018	-.158	.317	-.008	-.081
Bi	**.761**	.390	.100	-.062	-.165	.389	-.001	-.033	-.021
Ca	-.137	-.157	-.006	-.055	.058	**.832**	.053	.089	-.053
Cd	.053	-.020	.479	.179	-.074	.102	.123	.590	-.018
Ce	**.864**	-.189	.149	.080	-.082	-.022	.153	.060	-.074
Co	-.074	**.925**	-.059	.098	-.014	-.026	.104	.054	-.032
Cr	-.115	**.854**	-.089	.104	-.013	-.077	.027	-.003	-.019
Cu	.166	.007	.517	-.110	.149	-.186	.062	.329	.041
Fe	.417	**.799**	.040	.140	-.044	-.041	.162	.104	.057
Ga	**.935**	-.227	.056	-.029	-.077	-.057	-.036	.003	-.014
Ge	.093	.036	.535	.431	-.112	.066	-.029	.210	.054
Hg	-.253	-.113	.104	-.091	**.717**	-.192	-.037	-.120	.213
In	**.671**	.340	.108	-.019	.153	.314	.055	-.064	.147
K	**.843**	-.357	-.011	-.029	.060	-.116	-.082	-.033	-.215
La	**.818**	-.177	.214	.108	-.074	.018	.183	.080	-.068
Li	**.767**	.017	.160	.128	-.122	.083	.237	.111	.217
Mg	-.217	**.789**	-.048	-.233	-.115	.116	-.097	-.097	-.003
Mn	.186	.105	.254	.304	-.064	.036	**.726**	.209	.008
Mo	.278	-.054	.443	.212	.043	.083	.326	.106	-.139
Na	.066	-.162	-.088	-.116	.262	-.129	-.046	.002	**.761**
Nb	**.866**	-.011	-.054	.007	-.130	.010	-.024	-.026	.135
Ni	-.183	**.935**	-.050	.041	-.011	.007	.076	.037	-.067
P	.198	-.390	-.052	.211	-.066	-.042	.031	.114	.156
Pb	-.029	-.064	**.829**	.052	.158	-.042	.044	.084	.006
Rb	**.868**	-.261	.009	.001	-.029	-.100	-.005	-.050	-.228
S	-.202	-.231	.214	**.736**	.115	-.230	-.006	-.027	.002
Sb	-.116	-.055	.482	.226	.524	-.010	.111	-.211	.042
Sc	**.775**	.348	-.033	.006	-.129	-.048	.027	.060	.242
Se	**.772**	.395	.091	.032	-.182	.364	.068	-.031	-.047
Sn	.527	.163	.029	-.036	-.065	.179	-.061	-.082	-.062
Sr	.466	-.051	.097	.362	-.121	.394	-.039	-.086	.371
Ta	**.711**	.382	.078	.035	-.169	.344	.089	-.044	-.050
Te	.465	.255	-.008	-.041	.070	.571	.022	.076	-.118
Th	**.866**	-.223	.083	-.014	-.056	-.039	.051	-.003	-.210
Ti	**.882**	-.131	-.062	.007	-.125	-.032	-.029	-.015	.243
Tl	.051	.213	.083	**.721**	.062	.033	.177	.218	-.033
U	.464	.360	.078	.328	-.086	.235	-.235	-.035	.019
V	**.878**	.090	.045	.025	-.118	-.027	.053	.052	.237
W	.061	.120	.087	.092	.020	.024	**.710**	-.088	.000
Yt	**.729**	-.086	.196	.196	-.121	.029	.367	.176	.100
Zn	-.079	.000	.310	.101	.258	.087	-.035	**.759**	.000
Zr	**.642**	-.002	-.077	.060	-.208	.043	.171	.000	.430

Extraction Method: Principal Component Analysis.   Rotation Method: Varimax with Kaiser Normalization.

Table 3. Continued.
Rotated component matrix in second step.

	Component						
	1	**2**	**3**	**4**	**5**	**6**	**7**
Au	-.215	-.001	-.074	**.750**	.001	.261	.003
Ag	.151	-.045	.228	-.003	**.831**	.030	-.113
Al	**.952**	-.100	-.017	-.105	-.036	-.036	.059
As	-.225	-.027	.186	**.843**	.150	-.021	.017
Ba	.146	.011	**.767**	.062	.020	-.053	-.163
Be	**.697**	-.201	.227	-.066	-.068	-.134	-.023
Bi	**.752**	.435	-.039	-.146	.070	.362	-.071
Ca	-.112	-.148	.022	.138	-.009	**.872**	-.096
Ce	**.877**	-.151	.147	-.092	.137	-.027	-.067
Co	-.112	**.924**	.158	.001	-.042	-.035	-.045
Cr	-.158	**.842**	.111	-.008	-.083	-.097	-.034
Fe	.385	**.819**	.221	-.036	.047	-.052	.060
Ga	**.943**	-.187	-.049	-.093	.022	-.063	-.014
Hg	-.238	-.132	-.118	**.642**	.030	-.234	.233
In	**.673**	.375	.027	.155	.047	.293	.115
K	**.856**	-.322	-.096	.035	-.056	-.130	-.207
La	**.835**	-.139	.188	-.073	.184	.011	-.071
Li	**.771**	.046	.270	-.126	.166	.111	.235
Mg	-.251	**.797**	-.245	-.112	-.036	.109	-.028
Mn	.193	.098	**.725**	-.095	.296	.132	.101
Na	.074	-.156	-.116	-.109	-.120	.246	**.782**
Nb	**.866**	.037	-.025	-.135	-.067	-.006	.104
Ni	-.220	**.933**	.089	.004	-.023	-.004	-.074
Pb	.002	-.074	.116	.180	**.867**	-.095	-.005
Rb	**.877**	-.229	-.021	-.067	-.020	-.108	-.211
S	-.183	-.259	.584	.172	.129	-.368	-.114
Sc	**.753**	.376	.050	-.135	-.049	-.025	.244
Se	**.762**	.434	.082	-.166	.063	.345	-.089
Ta	**.703**	.421	.090	-.156	.051	.330	-.092
Th	**.878**	-.188	.003	-.080	.055	-.045	-.196
Ti	**.882**	-.087	-.019	-.140	-.079	-.041	.224
Tl	.054	.193	**.710**	.164	.048	-.014	-.085
V	**.871**	.126	.065	-.129	.031	-.020	.241
W	.056	.106	.492	-.111	.075	.077	.107
Yt	**.742**	-.057	.389	-.122	.209	.079	.144
Zn	-.043	.004	.150	.478	.448	.131	.004
Zr	**.638**	.034	.142	-.234	-.040	.064	.439

Extraction method: Principal component analysis. Rotation method: Varimax with Kaiser normalization.

Rotated component matrix in third step.

	Component						
	1	**2**	**3**	**4**	**5**	**6**	**7**
Au	-.206	.001	-.040	**.744**	-.009	.298	.000
Ag	.137	-.046	.231	-.008	**.850**	.061	-.097
Al	**.948**	-.105	.001	-.125	-.025	-.029	.088
As	-.222	-.024	.205	**.846**	.150	.017	.010
Ba	.122	.015	**.741**	.025	.065	-.002	-.100
Be	**.698**	-.203	.250	-.040	-.069	-.191	-.056
Bi	**.751**	.432	-.016	-.174	.081	.370	-.043
Ca	-.111	-.144	.027	.092	-.012	**.895**	-.077
Ce	**.871**	-.155	.188	-.095	.135	-.047	-.065
Co	-.112	**.924**	.161	-.005	-.048	-.044	-.045
Cr	-.151	**.846**	.077	.003	-.070	-.097	-.040
Fe	.380	**.818**	.228	-.051	.045	-.059	.069
Ga	**.943**	-.191	-.034	-.101	.033	-.059	.004
Hg	-.226	-.125	-.115	**.703**	.063	-.214	.202
In	**.675**	.377	.028	.141	.076	.318	.137
K	**.862**	-.323	-.074	.039	-.044	-.123	-.197
La	**.829**	-.143	.230	-.075	.181	-.010	-.071
Li	**.754**	.040	.298	-.153	.168	.100	.258
Mg	-.243	**.797**	-.233	-.104	-.039	.104	-.034
Mn	.170	.092	**.766**	-.098	.277	.050	.068
Na	.066	-.157	-.124	.251	-.093	-.104	**.792**
Nb	**.862**	.033	-.012	-.154	-.059	-.001	.130
Ni	-.219	**.933**	.101	-.002	-.035	-.014	-.076
Pb	-.007	-.071	.103	.184	**.888**	-.056	-.001
Rb	**.881**	-.231	-.002	-.066	-.009	-.108	-.202
Sc	**.745**	.371	.058	-.156	-.037	-.024	.272
Se	**.760**	.432	.092	-.198	.075	.350	-.061
Ta	**.701**	.419	.101	-.184	.062	.331	-.068
Th	**.879**	-.192	.042	-.077	.054	-.062	-.196
Ti	**.876**	-.091	-.018	-.162	-.066	-.033	.253
Tl	.020	.182	**.774**	.102	.026	-.002	-.031
V	**.862**	.121	.073	-.150	.043	-.018	.268
Yt	**.722**	-.065	.442	-.141	.195	.039	.147
Zr	**.622**	.029	.150	-.262	-.042	.048	.460

Extraction method: Principal component analysis. Rotation method: Varimax with Kaiser normalization.
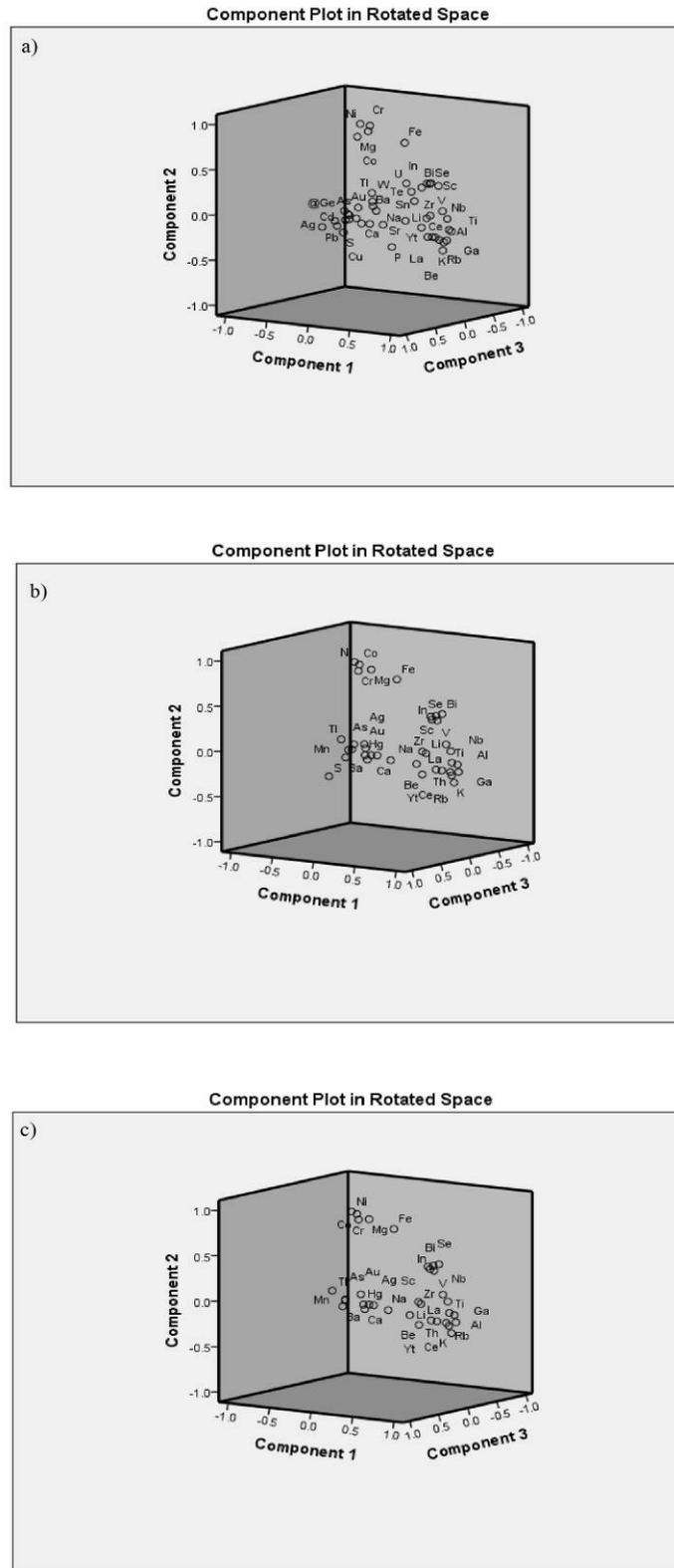
Figure 5. Component plot in rotated space in three steps of factor analysis: a) first; b) second; c) third.

Six geochemical populations for Au, five populations for As and Hg, and three populations for F4-3 were determined in the log-log plots that had a multi-fractal nature, as illustrated in Figure 6. Additionally, there are three main mineralized stages for Au, each can be sub-divided into two sub-stages: 1) Au values lower than 80 ppb; 2) Au values between 80 ppb and 1995 ppb; and 3) Au values higher than 1.995 ppm, which could be the main Au mineralized stage in the area, as

603

illustrated in Table 1. Furthermore, there is a positive correlation between Au and As, and, to a lesser amount, Hg (Figure 6). The populations below 80 ppb are the weakly mineralized stage, and between 0.08 and 1.995 ppm are the middle stages of Au mineralization. The middle and main Au mineralized stages occurred in the southern parts of the area (Figure 7).

The three main stages and three sub-stages of the Au mineralization [1-4] are correlated with the other elements due to the C-A fractal model, as depicted in Figure 7. The first stage of Au mineralization could be associated with the As values lower than 3467 ppm, Hg values below 1.78 ppm that contained an assemblage of early pyrrhotite, pyrite, and late chalcopyrite. The middle gold mineralization stage show a good correlation with the As concentrations between 3467 and 6409 ppm and Hg concentrations between 1.78 and 19 ppm. This stage is recognized by the widespread early base metal sulfides, lead-sulfosalts, and late zoned euhedral arsenical pyrite. The late stage is formed from network early arsenical pyrite, massive and colloform arsenical pyrite, colloform sphalerite, coloradoite, and late arsenic-antimony-mercury-thallium-bearing sulphides including the orpiment, realgar, stibnite, getchellite, cinnabar, lorandite, and a Tl-mineral, probably christite. Moreover, the main mineralized stage for Au had a good correlation with As and Hg higher than 6409 and 19 ppm, which occurred in the southern part of the area (Figure 7).

The log-log plot for the fourth factor of the third step (F4-3) obtained by the stepwise factor analysis consisting of Au, As, and Hg indicates three main stages: 1) the first stage that contains two sub-stages happenning in the F4-3 values lower than 1.2 2) middle stage comprising two sub-stages occurring in the factor values between 1.2 and 3.3 3) the final stage together with the two sub-stages have values higher than 3.3. The middle and main Au mineralized stages based on the stepwise factor analysis exist in the southern part of the studied area, as depicted in Figure 7. Therefore, six populations for Au are correlated with the three main mineralization stages, each composed of two sub-stages that are apparently reflected by the C-A plots in Figure 7.

Based on Asadi et al. (2000), gold occurs significantly in arsenical pyrite and colloform sphalerite as solid solution or as nanometer-sized native gold [2]. Metallic gold is found rarely in hydrothermal quartz and orpiment. Pure microcrystalline orpiment, carbon-rich shale,

silicified shale with visible pyrite grains, and arsenic minerals contain the highest concentrations of gold.

7. Comparison between results and geological particulars

At the Zarshuran gold deposit, the host sequences consist of the Chaldagh unit (argillaceous metalimestone) and the Zarshuran unit (carbonaceous black shale with silica and carbonate intercalations). Gold mineralization occurred as quartz-sulfide hydrothermal veins of massive quartz (jasperoid) and quartz veinlets formed by decalcification process along permeable horizons and high angle normal faults in the Chaldagh metalimestone. It also occurred as disseminations in the carbonaceous, siliceous, and calcareous beds of the Zarshuran black shale. Furthermore, the Miocene to Pliocene microdiorite intrusion [1-3], which is strongly fractured and altered, locally hosts some Au mineralization, and represents an association with the Neoproterozoic mineralized rocks.

The gangue minerals primarily consist of quartz, calcite, fluorite, hematite, and barite with accessory apatite, rutile, zircon, and xenotime (Table 1) [1-3]. Although micron-sized particles of gold are observed at Zarshuran, the quantities are insufficient to account for the assay grade, which has been shown to be due to the presence of invisible gold, particularly in pyrite, arsenian pyrite, and other sulphides [1-6].

8. Discussion

Gold mineralization in the Zarshuran Carlin-like deposit is spatially and genetically associated with the hydrothermally altered zones including the decarbonatization, argillic alteration, pervasive silicification, and sulfidation (Figure 2). There are associations of Au concentration with orpiment, realgar, arsenian pyrite, and cinnabar that are correlated with the results obtained by the stepwise factor analysis. There are gold mineralization with very fine-grained pyrite, massive orpiment, and realgar. The ore textures range from black breccias, brecciated jasperoid, and replacement/dissolution, typically occurring within the Chaldagh metalimestone and black gouge along the high-angle normal fault zones in the southern part of the deposit (Figure 7). In addition, there are proper values of porosity and permeability in host rocks that are increased by the removal of carbonate from the Chaldagh meta-limestone during the decarbonatization process. Furthermore, the intersection of high-angle

normal faults and fracture networks with Chaldagh meta-limestone and Zarshuran black shale generated suitable environment for gold and related elements' deposition. This process occurs in the southern part of the studied area that is correlated with the main anomalies of Au and related factors, as depicted in Figure 7.

Arsenic is one of the best pathfinder elements for the Carlin-like gold deposits [69-73]. The results

obtained indicate that the data obtained by the C-A fractal model and stepwise factor analysis strongly correlate with the Au mineralized stages and zones derived via geological data that show the major Au mineralization with As and Hg occurring along high angle normal faults that may act as conduits promoting fluid-flow and hydrothermal alterations in the southern part of the area.
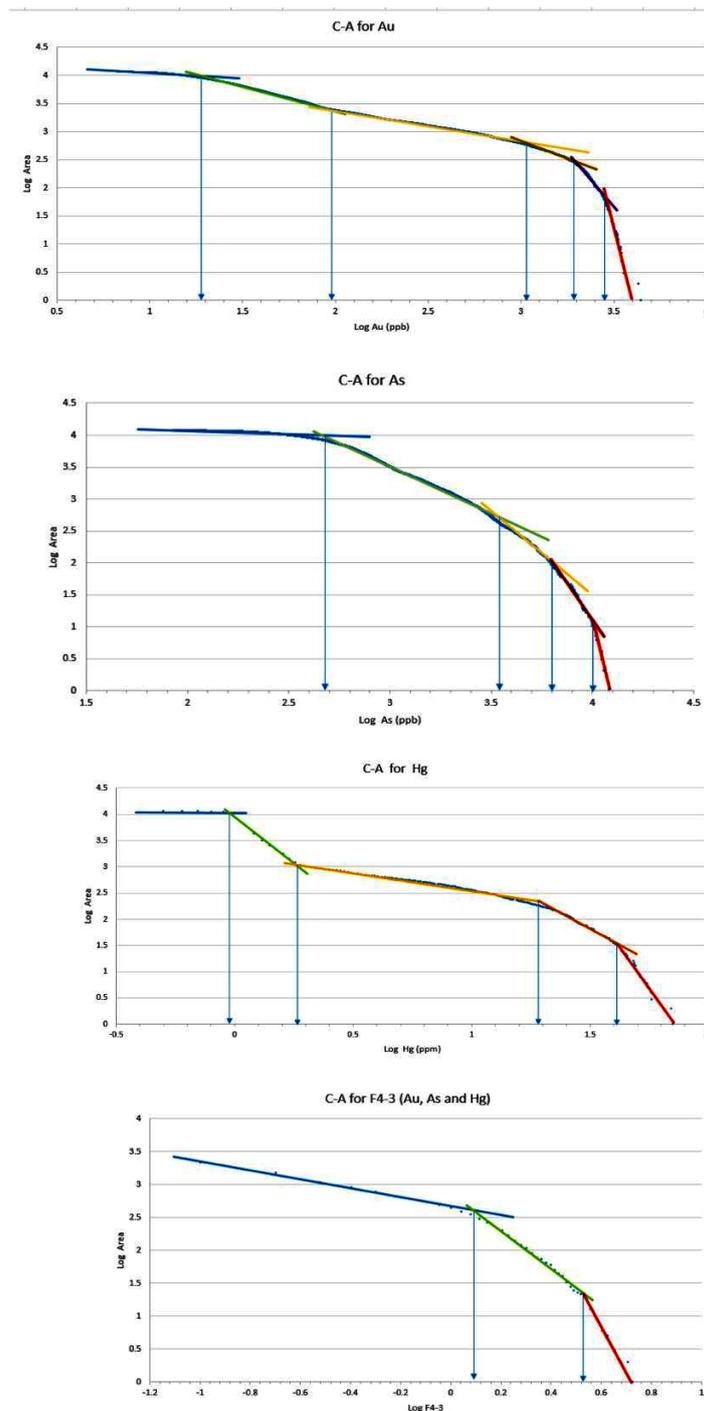
Figure 6. Au, As, Hg, and F4-3 C-A log-log plots.
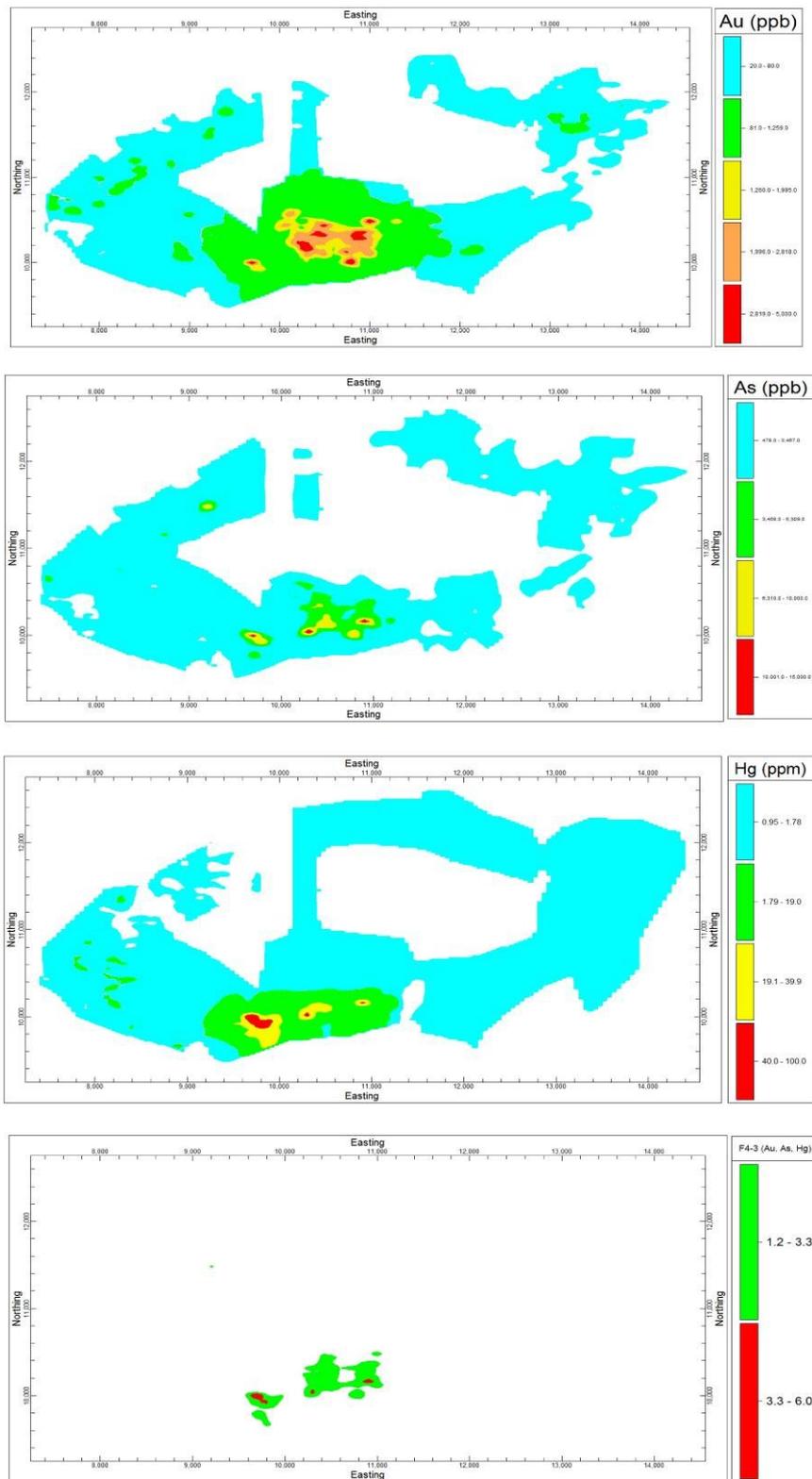
Figure 7. Au, As, and Hg geochemical population distribution maps based on C-A method.

9. Conclusions

The results of this work show that utilizing both the C-A fractal model and the stepwise factor analysis can improve the interpretation of litho-geochemical data for recognition of

mineralization stages. Based upon these results, there are three gold mineralization stages in the Zarshuran deposit that are correlated with the geological particulars. The stepwise factor analysis indicates that As and Hg are in the same

paragenesis with Au. The main stage of Au mineralization is located in the southern part of the area that contains arsenitic pyrites, cinnabar, and other sulfides in the silicic veins and black gouges. Favorable sedimentary sequences that are intersected by high-angle normal faults produced secondary permeability such as dissolution and brecciation, and veining played a major role in the localization of hydrothermal fluids and the formation of Zarshuran Carlin-like gold deposit. There are main environments for gold, arsenic, and mercury mineralization, especially in the southern part of the studied area. Moreover, these geological particulars confirm the results derived via the C-A fractal and stepwise factor analysis.

Delineation of the mineralization stages based on the C–A fractal model and stepwise factor analysis could be of important help to geoscientists for interpreting the stages in which an element is enriched in a deposit. Additionally, using the fractal/multifractal modeling and factor analysis could be proposed as a new approach for the interpretation of the litho-geochemical data in geochemical exploration and economic geology.

Acknowledgments

References

[1]. Mehrabi, B., Yardley, BWD. and Cann, J.R. (1999). Sediment-hosted disseminated gold mineralisation at Zarshuran, NW Iran. Miner. Dep. 34: 673-696.

[2]. Asadi, H.H., Voncken, J.H.L. and Hale, M. (2000). Invisible gold at Zarshuran, Iran. Econ. Geol. 94: 1367-1374.

[3]. Daliran, F., Hofstra, A., Walther, J. and Stuben, D. (2002). Aghdarreh & Zarshuran SRHGD deposits, Takab region, NW-Iran [abs.]. Geol. Soc. of America. Abstracts with programs. 34 (6): 141.

[4]. Richards, J.P., Wilkinson, D. and Ulrich, T. (2006). Geology of the Sari Gunay Epithermal Gold Deposit, Northwest Iran. Econ. Geol. 101: 1455-1496.

[5]. Richards, J.P. (2013). Mineralization styles and orogen spisodes in the Tethyan. Soc. of Geol. Scienc. Amer. 1408-1411.

[6]. Daliran, F. (2008). The carbonate rock-hosted epithermal gold deposit of Agdarreh, Takab geothermal field, NW Iran, hydrothermal alteration and mineralization. Miner. Dep. 43: 383-404.

[7]. Anglo American Exploration Co. (2001). Final Technical Report, Zarshuran Gold Project. Final report, Ministry of Industry and Mine.

[8]. Kavoshgaran Consultant Engineering Co. (2012). Preliminary report for the estimation of ore reserve in the Zarshuran gold deposit. Internal report in Persian. 150 P.

[9]. Aliyari, F., Abdollahi Sharif, J. and Fadaei, M.J. (2013). Geological maps and 3D modeling of gold deposits and their exploration guides: Zarshuran gold deposit. 1st 3D Geological Modeling Conference, Geol. Surv. of Iran pp. 1-2.

[10]. Mehrabi, B. (2008). Solid solution in the As_2S_3-Sb_2S_3 series at Zarshuran gold deposit, Iran. J. of Sci. I.R. I. 19 (2): 137-143.

[11]. Asadi, H.H., Voncken, J.H.L., Kuhnel, R.A. and Hale, M. (2000). Petrography, mineralogy and geochemistry of the Zarshuran Carlin-like gold, Miner. Dep. 35: 656-671.

[12]. Asadi, H. and Hale, M. (2006). A predictive GIS model for potential mapping of gold and base metal mineralization in Takab area, Iran. Int. Inst. for Aero. Surv. and Ear. Scie, (ITC). Netherlands (ppt).

[13]. Mandelbrot, B.B. (1983). The fractal geometry of Nature. W.H Freeman. San Francisco. 468 P.

[14]. Turcotte, D.L. (1986). A fractal approach to the relationship between ore grade and tonnage. Econ. Geol. 18: 1525-1532.

[15]. Agterberg, F.P., Cheng, Q. and Wright, DF. (1993). Fractal modeling of mineral deposits. In: Elbrond, J., Tang, X., (Eds.). 24th APCOM Symp. Proceed., Mont., Can. pp. 43-53.

[16]. Cheng, Q., Agterberg, F.P. and Ballantyne, S.B. (1994). The separation of geochemical anomalies from background by fractal methods. J. of Geoch. Explor. 51: 109-130.

[17]. Cheng, Q. (1999). Spatial and scaling modeling for geochemical anomaly separation. J. of Geoch. Explor. 65 (3): 175-194.

[18]. Sim, B.L., Agterberg, F.P. and Beaudry, C. (1999). Determining the cutoff between background and relative base metal contamination levels using multifractal methods. Comp. & Geosc. 25: 1023-1041.

[19]. Goncalves, M.A., Mateus, A. and Oliveira, V. (2001). Geochemical anomaly separation by multifractal modeling. J. of Geoch. Explor. 72: 91-114.

[20]. Shen, W. and Zhao, P. (2002). Theoretical study of statistical fractal model with applications to mineral resource predition. Comp. & Geosc. 28: 369-376.

[21]. Li, C., Ma, T. and Shi, J. (2003). Application of a fractal method relating concentrations and distances for separation of geochemical anomalies from background. J. of Geoch. Explor. 77: 167-175.

[22]. Carranza, E.J.M. (2009). Objective selection of suitable unit cell size in data-driven modeling of mineral prospectivity. Comp. & Geosc. 35: 2032-2046.

[23]. Carranza, E.J.M. (2011). Analysis and mapping of geochemical anomalies using logration-transformed stream sediment data with censored values. J. of Geoch. Explor. 110: 167-185.

[24]. Zou, R., Cheng, Q. and Xia, Q. (2009). Application of fractal models tocharacterization of vertical distribution of geochemical ele-ment concentration. J. of Geoch. Explor. 102 (1): 37-43.

[25]. Zuo, R., Carranza, E.J.M. and Cheng, Q. (2012). Fractal/multifractal modeling of geochemical exploration data. J. of Geoch. Explor. 122: 1-3.

[26]. Afzal, P., Khakzad, A., Moarefvand, P., Rashidnejad Omran, N., Esfandiari, B. and Fadakar Alghalandis, Y. (2010). Geochemical anomaly separation by multifractal modeling in Kahang (Gor Gor) porphyry system, Central Iran. J. of Geoch. Explor. 104: 34-46.

[27]. Afzal, P., Dadashzadeh Ahari, H., Rashidnejad Omran, N. and Aliyari, F. (2013). Delineation of gold mineralized zones using concentration-volume fractal model in Qolqoleh gold deposit, NW Iran. Ore Geol. Rev. 55: 125-133.

[28]. Carranza, EJM. and Sadeghi, M. (2010). Predictive mapping of prospectivity and quantitative estimation of undiscovered VMS deposits in Skellefte district (Sweden). Ore Geol. Rev. 38: 219-241.

[29]. Wang, G., Zhang, S., Yan, C., Song, Y., Ma, Z. and Li, D. (2011). 3D geological modeling based on geological and gravity-magnetic integration in Luanchuan molybdenum polymetallic region, China. Earth Sciences. J. of China Univ. of Geosc. 36: 266-360.

[30]. Zuo, R. (2011). Decomposing of mixed pattern of arsenic using fractalmodel in Gangdese belt, Tibet, China. Appl. Geoch. 26: 271-73.

[31]. Zuo, R. (2011). Identifying geochemical anomalies associated with Cu and Pb-Zn skarn mineralization using principal component analysis and spectrum-area fractal modeling in the Gangdese belt, Tibet (China). J. of Geoch. Explor. 111: 13-22.

[32]. Arias, M., Gumiel, P. and Martin-Izard, A. (2012). Multifractal analysis of geochemical anomalies: a tool for assessing prospectivity at the SE border of the Ossa Morena Zone, Variscan Massif (Spain). J. of Geoch. Explor. 122: 101-112.

[33]. Heidari, M., Ghaderi, M. and Afzal, P. (2013). Delineation mineralized phases based on lithogeochemical data using multifractal model in Tuzlar epithermal Au-Ag (Cu) deposit, NW Iran. Appl. Geoch. 31: 119-132.

[34]. Chandrajith, R., Dissanayake, C.B. and Tobschall, H.J. (2001). Application of multi-element relationships in stream sediments to mineral exploration: a case study of Walawe Ganga basin, Sri Lanka. Appl. Geoch. 16 (3): 339-350.

[35]. Kumru, M.N. and Bakac, M. (2003). R-mode factor analysis applied to the distribution of elements in soils from the Aydin basin, Turkey. J. of Geoch. Explor. 77: 81-91.

[36]. Reimann, C., Filzmoser, P. and Garrett, R.G. (2005). Background and threshold. critical comparison of methods of determination. Sci. of the Tot. Environ. 346: 1-16.

[37]. Grunsky, E.C., Drew, L.J. and Sutphin, D.M. (2009). Process recognition in multi-element soil and stream-sediment geochemical data. Appl. Geoch. 24 (8): 1602-1616.

[38]. Yousefi, M., Kamkar-Rouhani, A. and Carranza, E.J.M. (2012). Geochemical mineralization probability index (GMPI): a new approach to generate enhanced stream sediment geochemical evidential map for increasing probability of success in mineral potential mapping. J. of Geoch. Explor. 115: 24-35.

[39]. Johnson, R.A. and Wichern, D.W. (2002). Applied multivariate statistical analysis. 5th eds. Prentice Hall. Upper Saddle River.

[40]. Babakhani, A. and Ghalamghash, J. (1990). Geological map of Takhte Soleyman (1/100000). Geol. Surv. of Iran.

[41]. Alavi, M. (1994). Tectonic of the Zagros orogenic belt of Iran: new data and interpretations, Tectonoph. 229: 211-238.

[42]. Mohajjel, M., Fergusson, C.L. and Sahandi, M.R. (2003). Cretaceous–Tertiary convergence and continental collision, Sanandaj-Sirjan zone, western Iran. J. of Asi. Ear. Scien. 21: 397-412.

[43]. Mohajjel, M. and Fergusson, C.L. (2014). Jurassic to Cenozoic tectonics of the Zagros Orogen in northwestern Iran, Intern. Geol. Rev. 56 (3): 263-287.

[44]. Rabiei, A., Kousari, S. and Hosseini, M. (2006). Alteration, mineralization, and genesis of Touzlar gold deposit, Iran. Proceedings of the 24th Symposium on Geosciences, Geological Survey of Iran, Tehran, Iran. (in Persian with English abstract, CD-ROM).

[45]. Hitzman, M.W., Reynolds, N.A., Sangster, D.F., Allen, C.R. and Carman, C.E. (2003). Classification,

gensis, and exploration guides for nonsulfide zinc deposits. Econ. Geol. 98: 685-714.

[46]. Gilg, H.A., Allen, C., Balassone, G., Boni, M. and Moore, F. (2003). The 3-stage evolution of the Agouran Zn "oxide"-sulfide deposite, Iran. In: Eliopoulos D et al (eds) Mineral exploration and sustainable development. Millpress. Rotterdam. pp. 77-80.

[47]. Borg, G. and Daliran, F. (2004). Hypogene and supergene formation of sulfides and non-sulfides at the Angouran high-grade Zinc deposit, NW Iran. In: Abstract Volume of Geoscience Africa 2004. University of the Witwatersrand. Johannesburg. pp. 69-70.

[48]. Daliran, F., Pride, K., Walther, J., Berner, Z.A. and Bakker, R.J. (2013). The Angouran Zn (Pb) deposit, NW Iran: Evidence for a two stage, hypogene zinc sulfide-zinc carbonate mineralization. Ore Geol. Rev. 53: 373-402.

[49]. Zanjani, A. (1945). Bayche-Bagh Copper mine. Open file report, Ministry of Mines and Metals of Iran. Tehran. 15 P.

[50]. Lotfi, M. and Karimi, M. (2004). Ggeology, mineralogy and ore genesis of Byche-Bagh (Ni-Co-As-Bi and base metals) vein-type deposit (NW Zanjan, Iran). Abstract volume of the 32nd Inter. Geol. Cong. (part 2, abstract 215-34).

[51]. Shirkhani, M. (2007). Geology, mineralogy, and geochemistry of Ay Qalesi Zn-Pb-Cu deposit, Takab area. Unpublished MSc Thesis. Tarbiat Modares University. Tehran. Iran. 245 P.

[52]. Mohajer, G.H., Parsaie, H., Fallah, N. and Madani, F. (1989). Mercury exploration in the Saein Dez- Takab. Ministry of Mines and Metals of Iran. Tehran [in Persian].

[53]. Mehrabi, B., Yardley, B.W.D. and Komninue, A. (2003). Modeling the As-Au association in hydrothermal gold mineralization: Example of Zarshuran deposit, NW Iran. J. of Scien. Islam. Rep. of Iran. 14 (1): 37-52.

[54]. Karimi, M. (1992). Geology, petrography and mineralogical studies of Zarshuran gold deposit, Kans. Engin. Comp. Tehran. Iran.

[55]. Lima, A., De Vivo, B., Cicchella, D., Crotini, M. and Albanese, S. (2003). Multifractal IDW interpolation and fractal filtering method in environmental studies: an application on regional stream sediments of (Italy), Campania region. Appl. Geoch. 18: 1853-1865.

[56]. Halsey, T.C., Jensen, M.H., Kadanoff, L.P., Procaccia, I. and Shraiman, B.I. (1986). Fractal measures and their singularities: the characterization of strange sets. Phys. Rev. A. 33 (2): 1141-1151.

[57]. Evertsz, C.J.G. and Mandelbrot, B.B. (1992). Multifractal measures (appendix B). In: Peitgen, H.O., Jurgens, H. and Saupe, D. (Eds.). Chaos and fractals. Springer. New York.

[58]. Bolviken, B., Stokke, P.R., Feder, J. and Jossang, T. (1992). The fractal nature of geochemical landscapes. J. of Geoch. Explor. 43: 91-109.

[59]. Turcotte, D.L. (1997). Fractals and chaos in geology and geophysics. Cambridge University Press. 398 P.

[60]. Cheng, Q. and Agterberg, F.P. (1996). Multifractal modeling and spatial statistics, Math. Geol. 28 (1): 1-16.

[61]. Davis, J.C. (2002). Statistics and data analysis in geology. 3rd edition. John Wiley & Sons Inc. New York.

[62]. Kaiser, H.F. (1958). The varimax criterion for analytic rotation in factor analysis. Psychometrika. 23: 187-200.

[63]. Yousefi, M. and Carranza, E.J.M. (2015). Fuzzification of continuous-value spatial evidence for mineral prospectivity mapping. Comp & Geosci. 74: 97-109.

[64]. Yousefi, M. and Carranza, E.J.M. (2015). Prediction-area (P-A) plot and C-A fractal analysis to classify and evaluate evidential maps for mineral prospectivity modeling. Comp & Geosci. 79: 69-81.

[65]. Yousefi, M. and Carranza, E.J.M. (2015). Geometric average of spatial evidence data layers: A GIS-based multi-criteria decision-making approach to mineral prospectivity mapping. Comp & Geosci. 83: 72-79.

[66]. Yousefi, M. and, Nykänen, V. (2016). Data-driven logistic-based weighting of geochemical and geological evidence layers in mineral prospectivity mapping. J. Geochem Explor. 164: 94-106.

[67]. Cheng, Q. (2008). Modeling local scaling properties for multiscale mapping. Vad. Zone J. 7: 525-532.

[68]. David, M. (1970). Geostatistical ore reserve estimation. Elsevier. Amsterdam. 283 P.

[69]. Stenger, D.P., Kesler, S.E., Peltonen, D.R. and Tapper, C.J. (1998). Deposition of gold in carlin-type deposits; the role of sulfidation and decarbonation at Twin Creeks, Nevada. Economic Geology, 93(2), 201-215.

[70]. Theodore, T.G., Kotlyar, B.B., Singer, D.A., Berger, V.I., Abbott, E.W. and Foster, A.L. (2003). Applied geochemistry, geology, and mineralogy of the northernmost Carlin trend, Neveda. Econ. Geol. 98: 287-316.

[71]. Cline, J.S., Hofstra, A.H., Muntean, J.L., Tosdal, R.M. and Hickey, K.A. (2005). Carlin-type gold

deposits in Nevada: Critical geologic characteristics and viable models. Economic Geology 100th anniversary volume. 100: 451-484.

[72].Bettles, K. (2002). Exploration and geology, 1962 to 2002, at the Goldstrike property, Carlin trend, Nevada. Special publication-society of economic geologists. 9: 275-298.

[73]. Carranza, E.J.M., Owusu, E.A. and Hale, M. (2009). Mapping of prospectivity and estimation of number of undiscovered prospects for lode gold, southwestern Ashanti Belt, Ghana. Mineralium Deposita. 44 (8): 915-938.

تعیین و جدایش آنومالی‌های ژئوشیمیایی و مراحل کانه‌زایی بر اساس داده‌های لیتوژئوشیمیایی در کانسار تیپ شبه کارلین زرشوران (شمال غرب ایران) با استفاده از مدل‌سازی چندفرکتالی و آنالیز فاکتوری مرحله‌ای

فرهنگ علیاری[۱]*، پیمان افضل[۲] و جعفر عبدالهی شریف[۱]

۱- گروه مهندسی معدن، دانشگاه صنعتی ارومیه، ایران

۲- بخش مهندسی معدن، دانشگاه آزاد اسلامی، واحد تهران جنوب، ایران

۳- گروه مهندسی معدن، دانشگاه ارومیه، ایران

* نویسنده مسئول مکاتبات: f.aliyari@uut.ac.ir

چکیده:

کانسار طلای زرشوران از نوع شبه کارلین در کمربند فلززایی تکاب و نیز در بخش شمالی زون سنندج- سیرجان قرار دارد. بخش‌های پـر عیـار مـاده معـدنی درون شیل‌های سیاه و آهک‌های کرم تا خاکستری رنگ و در امتداد گسل‌های کششی و زون‌های ساختاری با رونـد شـمال و شـمال غربـی وجـود دارنـد. هـدف از ایـن پژوهش جدایش مراحل کانه‌زایی طلا بر اساس میزان عیارهای طلا، جیوه و آرسنیک حاصـل از داده‌هـای لیتوژئوشـیمیایی سـطحی بـا اسـتفاده از روش فرکتـالی عیار- مساحت و آنالیز فاکتوری مرحله‌ای در کانسار زرشوران است. بر اساس روش‌های ذکرشده سه مرحله کانه‌زایی برای طلا در این کانسار بـه دسـت آمـد کـه بـا داده‌ها و مطالعات زمین‌شناسی مطابقت داده شدند. مرحله اصلی کانه‌زایی طلا که از عیار ۱/۹۵۵ گرم در تن برای طلا، ۶۴۰۹ و ۱۹ گرم در تـن بـرای آرسـنیک و جیوه آغاز می‌شود با مرحله اصلی سولفیدشدگی و نیز رگه/ رگچه‌های سولفید کوارتز همراه است. همچنین نتایج حاصل از مدل‌سـازی فرکتـالی و آنـالیز فـاکتوری مرحله‌ای در تطبیق با مشخصات زمین‌شناسی نشان می‌دهد که بخش اصلی کانه‌زایی طلا در بخش جنوبی کانسار زرشوران اتفاق افتاده است.

کلمات کلیدی: آنومالی لیتوژئوشیمیایی، روش فرکتالی عیار- مساحت، آنالیز فاکتوری مرحله‌ای، زرشوران.